Impact of bivariate energy and angular atomic impact spectra on tungsten erosion in JET

OPEN ACCESS
IOP Publishing
Plasma Physics and Controlled Fusion
Plasma Phys. Control. Fusion **67** (2025) 055044 (8pp)
https://doi.org/10.1088/1361-6587/add376

Impact of bivariate energy and angular atomic impact spectra on tungsten erosion in JET

H A Kumpulainen[1,*], D Reiter[2], S Brezinsek[1], M Groth[3], J Romazanov[1], S Wiesen[4] and the JET contributors[5]

[1] Forschungszentrum Jülich GmbH, Jülich, Germany
[2] Heinrich-Heine-Universität Düsseldorf, Düsseldorf, Germany
[3] Aalto University, Espoo, Finland
[4] Dutch Institute for Fundamental Energy Research, Eindhoven, The Netherlands

E-mail: h.kumpulainen@fz-juelich.de

Received 11 February 2025, revised 19 April 2025
Accepted for publication 2 May 2025
Published 13 May 2025

Abstract

The erosion of tungsten plasma-facing components due to charge-exchange atoms, predicted to be the dominant cause of the observed W radiation in most JET plasmas with a Be/W wall (formerly ITER-like wall), is quantified by the first EIRENE simulations of the bivariate energy-angular impact spectrum and the incident flux of deuterium and tritium atoms. The tungsten erosion rate due to the bivariate impact spectrum in the JET outer vertical divertor corresponds to a constant effective impact angle of 43°. Assuming independent univariate energy and angular distributions instead of the bivariate spectrum causes a predicted increase of order 10% in the tungsten influx and the core radiated power. The predicted tungsten sputtering rate due to tritium atoms is 2–6 times the sputtering rate by deuterium atoms in similar edge plasmas. A hypothetical replacement of all JET first-wall materials with tungsten is predicted to raise the total radiated power by 60% in a diverted H-mode scenario if the added radiation is offset by additional heating and the plasma conditions are unchanged.

Supplementary material for this article is available online

Keywords: sputtering, tungsten, functional expansion tallies, deuterium, tritium, charge exchange, Monte Carlo

[5] See Maggi *et al* 2024 (https://doi.org/10.1088/1741-4326/ad3e16) for the JET contributors.
[*] Author to whom any correspondence should be addressed.

1. Introduction

The erosion of plasma-facing components (PFCs) in fusion devices presents significant challenges and operational limitations, such as the duty cycle of PFCs, plasma contamination by impurities, and increased tritium retention in co-deposits [1–3]. The choice of tungsten (W) as a plasma-facing material combined with detached plasma operation has the potential to effectively suppress the erosion caused by ions at the divertor targets [4]. However, W erosion is not only caused by ions but also neutral atoms, particularly charge-exchange neutrals (CXNs), which are created when single-charged ions undergo charge exchange with atoms and molecules in the edge plasma [5, 6].

Integrated core-edge simulations with interpretive plasma conditions and predictive W erosion and transport have demonstrated that the predicted W sputtering by fuel atoms is sufficient to account for virtually all the W measured in the core plasma in JET L-mode and H-mode plasmas [7]. The CXN initial energies are proportional to the ion temperature at the source location, but unlike ions, CXNs are not confined by magnetic fields and in many cases reach the wall without thermally equilibrating with the colder plasma near the wall surfaces [6]. Hence, CXN fluxes with sufficient energy induce sputtering from all surfaces within the line of sight, including areas that lack the efficient impurity screening observed at the divertor targets [2]. In attached JET plasmas, the CXN contribution to the gross erosion of W is predicted to be negligible at the strike lines, but dominant on the W-coated tiles near the low-field side divertor entrance and in the main chamber [7].

The following research questions are addressed in this paper:

(1) How does the correlation between atomic impact energy and angle affect W erosion in JET?
(2) How does W erosion by atoms differ between deuterium (D) and tritium (T) JET plasmas?
(3) How is the total power radiated by W affected by the incident atomic distribution?
(4) Consistent with the updated ITER baseline changing to a W first wall [8], what is the predicted rate of W erosion and influx due to D atoms from a hypothetical W JET main chamber [9]?

The plasma scenarios presented (low-density L-mode, $B_\mathrm{T} = 2.5$ T, $I_\mathrm{p} = 2.5$ MA, $P_\mathrm{aux} = 1$ MW and intermediate-density type-I ELMy H-mode, $B_\mathrm{T} = 2.5$ T, $I_\mathrm{p} = 2.3$ MA, $P_\mathrm{aux} = 18$ MW) are based on previous studies with available validated background plasma modelling [10, 11]. Both scenarios use the vertical-horizontal divertor target configuration (figure 1). The main advantage of studying JET plasmas as opposed to future devices is the availability of measurement data for the validation of the simulated plasma conditions and for assessing the plausibility of the predicted W erosion and influx.

2. Methods

The bivariate atomic impact energy and angular distribution, including CXN, reflected and recycled atoms from the walls, and atoms created in the plasma volume by recombination and dissociation processes, is simulated using the 3D Monte Carlo kinetic neutral transport code EIRENE [13]. The tally surfaces selected for this study are segments of the axisymmetric wall contour as indicated in figure 1. EIRENE provides the option of defining arbitrary diagnostic surfaces to further enhance the spatial resolution of the atomic distribution, but opting for fewer and larger surfaces reduces the statistical noise in the predictions.

Contrary to previous EIRENE studies on CXN and W erosion [7, 14] which neglected the correlation between univariate energy and angular impact spectra, this study demonstrates the first application and verification of a newly implemented tallying method for bivariate energy-angular spectra. Instead of conventional histogram binning, the distribution of polar impact angles is recorded using functional expansion tallies (FET) [15, 16] with a Legendre polynomial basis. Legendre polynomials have been used here because they describe the angular distribution (polar angle) in spherical coordinates. EIRENE computes the Legendre polynomial expansion coefficients a_n up to a user-specified degree d for the impact angle cosines within each energy bin. As the polar impact angle cannot exceed 90° but the Legendre polynomials are orthonormal over the interval $[-1, 1]$, the impact angle cosines are uniformly projected from the range $[0, 1]$ to $[-1, 1]$ for improved convergence of the polynomial series.

The polar angle distribution $f(\theta)$ for each energy bin is reconstructed in post-processing from the Legendre expansion coefficients (equation 1):

$$f(\theta) = \sum_{n=0}^{d} a_n \cdot \pi \sin(\theta) \cdot L_n(2\cos(\theta) - 1). \tag{1}$$

L_n is the Legendre polynomial of degree n. The primary advantage of the FET method over histogram tallying is that every particle trajectory contributes to the full angular distribution as opposed to a single angular bin, avoiding the compromise between high angular resolution (many bins) and low stochastic variance (many particles per bin). The obtained polynomial expansion therefore achieves, on average, higher accuracy for the same amount of particles than a histogram. The polynomials are also infinitely smooth and differentiable, and the distribution can be evaluated at arbitrarily high resolution in post-processing.

The simulations presented use 15 energy bins from 1 eV to 10 keV with logarithmic energy intervals. The 10th degree Legendre expansion is computed for the impact angle cosines. Bivariate energy-angular histogram tallies are also computed for comparison and verification of the FET method.

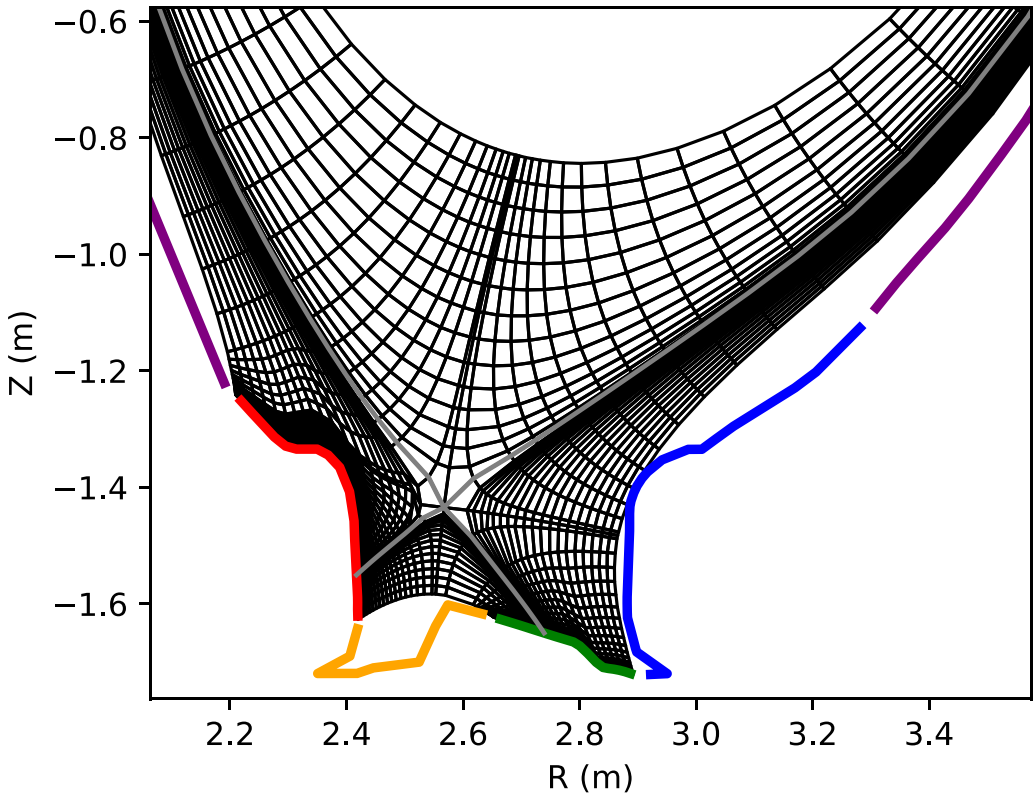

Figure 1. Geometry of the EDGE2D-EIRENE [12] computational domain (black) in the vertical-horizontal divertor configuration for JET discharge #81472 at 9 s. The contour of the JET tungsten divertor components is divided into regions which are referred to as the inner target (red), the private flux region (orange), the outer target (green), and the outer vertical divertor (blue). The beryllium main chamber wall contour is indicated in purple and the separatrix in gray.

3. Application of functional expansion tallies to JET simulations

3.1. Angular impact spectra of D and T atoms in JET L-mode and H-mode plasmas

The correct implementation and post-processing of the functional expansion tallies in EIRENE is verified by comparison with a histogram of the angular spectrum (figure 2). The bin interval is non-uniform in angular space because the binning is carried out on the impact angle cosines rather than the angles. The angles are defined relative to the surface normal such that an angle of 0° indicates perpendicular impact and 90° is tangential. Functional expansion tallies demonstrate both higher angular resolution and lower statistical noise than histogram tallies for the same particle trajectories. The measured and simulated EDGE2D-EIRENE plasma profiles along the low-field side mid-plane and the low-field side target are attached as supplementary data.

For D atoms with low impact energies, originating primarily in the cold scrape-off layer (SOL) regions adjacent to the wall, the polar impact angles approximately follow a cosine distribution with a weak bias towards shallower impact angles (figure 3(a)). In contrast, the angular distribution of atoms with impact energies of several hundred eV, above the W sputtering threshold, is skewed towards steeper angles with a maximum near 40° with respect to the surface normal (figure 3(c)).

3.2. W erosion by CXN in D and T plasmas

The rate of W gross erosion due to D atom impact is calculated by multiplying the D flux and the impact energy and angular distribution with the W sputtering yield corresponding to each combination of impact energy and angle (figure 4). The sputtering yields are based on SDTrimSP6 [17] simulations.

Applying the univariate energy spectrum with a constant effective incidence angle of 43°, as an approximation of the bivariate atomic impact distribution, yields a similar total flux of sputtered W, but not the same dependence of the eroded W flux on impact energy, compared to the fully resolved bivariate energy-angular distribution (figure 4). Integrating the bivariate distribution over the impact angles and neglecting the correlation between impact energy and angle ('energy-independent angles', red), the obtained W erosion rate is accurate to within 5% of the fully angle-resolved calculation ('fully resolved angles', green) at impact energies below 600 eV but overestimated by 30%–50% at $E > 2$ keV. Assuming a normal incidence causes a significant underestimate of the W erosion at all impact energies.

The predicted gross erosion rate of W due to atoms is higher in a T plasma than in a D plasma by a factor of 4–6 in the L-mode and inter-ELM (figure 5(a)) scenarios and by a factor of 2–3 during type-I ELMs (figure 5(b)). The maximum W erosion rate from the outer vertical divertor (OVD) during the ELM phase exceeds the inter-ELM rate by more than two

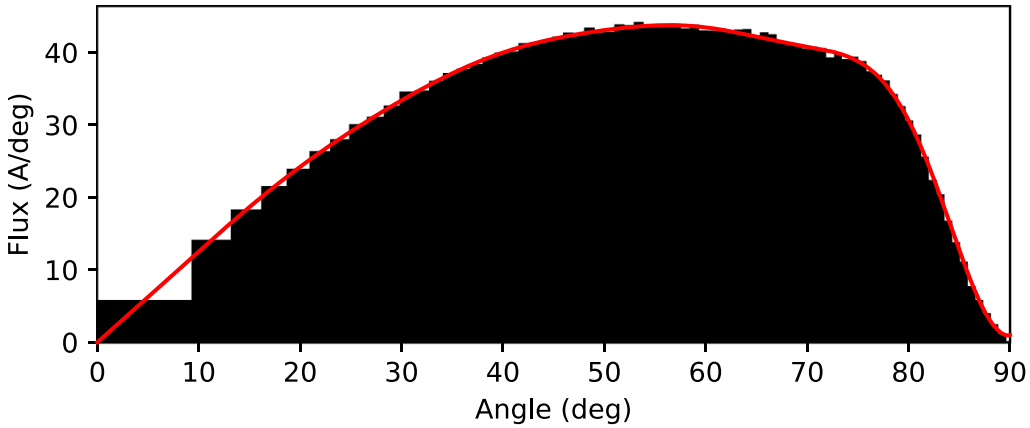

Figure 2. Polar angle distribution of D atoms incident on the JET main chamber wall (see figure 1 for wall region definitions) predicted by EIRENE in L-mode discharge #81472 at 9 s, integrated over all impact energies. Functional expansion tallies are shown in red and histogram tallies with 75 bins in black.

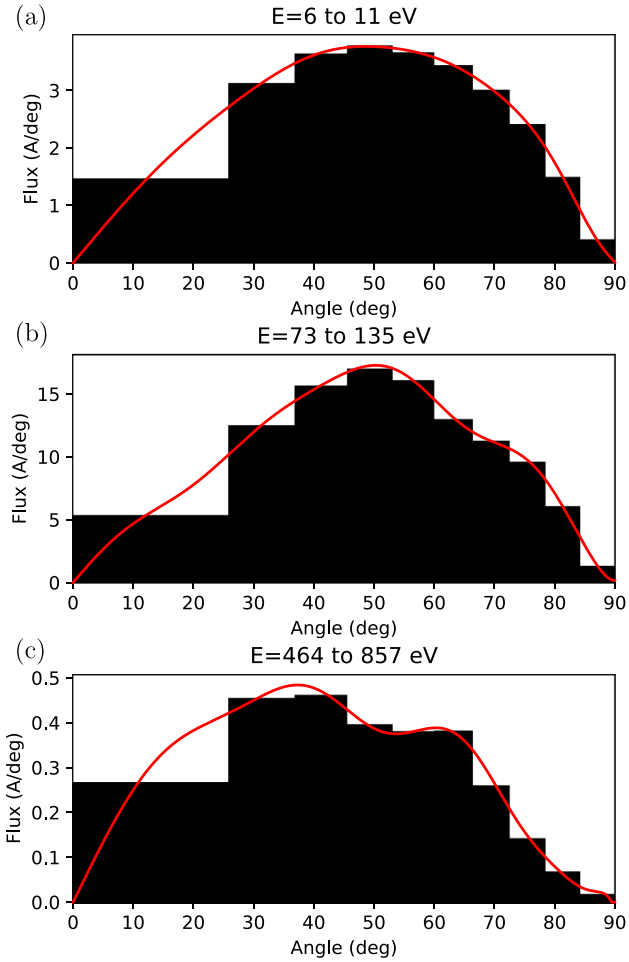

Figure 3. Polar angle distribution of D atoms incident on the outer vertical divertor predicted by EIRENE in JET L-mode discharge #81472 at 9 s for three energy ranges corresponding approximately to the ion temperatures in the far-SOL (a), at the separatrix (b) and in the confined plasma at normalized minor radius 0.9 (c). Functional expansion tallies are shown in red and histogram tallies with 10 bins in black.

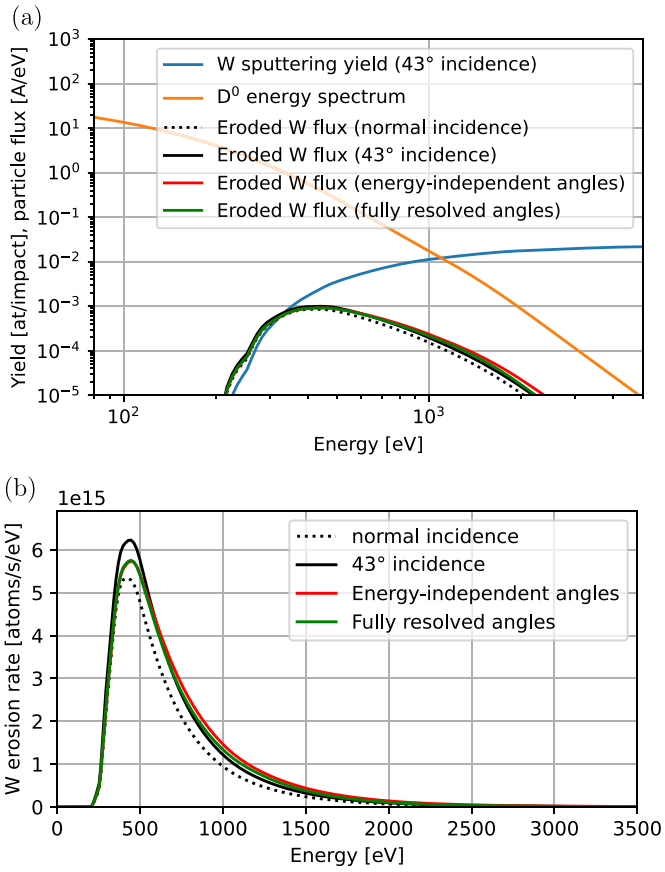

Figure 4. (a) The W sputtering yield by D (SDTrimSP), the D^0 impact energy spectrum (EIRENE), and the resulting flux of eroded W as a function of the D impact energy based on different assumptions on the impact angle distribution at the outer vertical divertor in JET L-mode discharge #81472 at 9 s. (b) The same fluxes of eroded W as in (a), but converted to units of atoms/s/eV and shown on a linear scale.

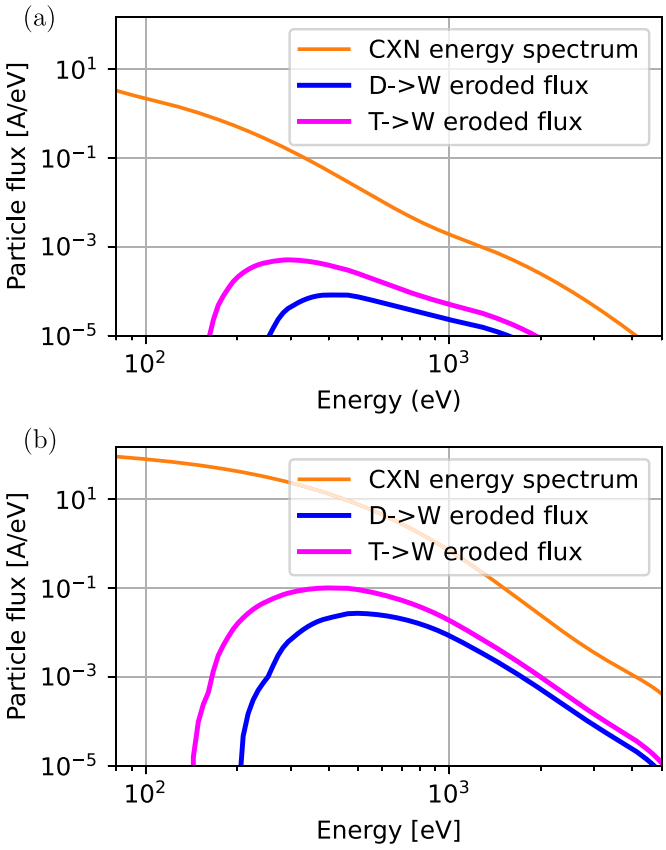

Figure 5. Energy spectrum of incident atoms and the eroded flux of tungsten as a function of impact energy in the outer vertical divertor assuming deuterium (blue) and tritium (magenta) as the incident atom species, and identical edge plasma conditions in D and T, based on the (a) inter-ELM phase and (b) peak heat flux during the ELM phase of JET H-mode discharge #94606 at 10–11 s.

orders of magnitude, not only due to higher CXN impact energies but to a large extent fast reflections of keV-range ions from the LFS divertor target. It is assumed that control parameters such as the fueling rate and heating power are adjusted to obtain equal electron and ion densities and temperatures in the edge plasma between the D and T scenarios. This assumption leads to similar energy and angular distributions of the incident D and T atoms. Experimentally, achieving similar density and temperature in D and T is expected to require several iterations of optimizing the control parameters, which has not been done for these scenarios. The increased W sputtering in T compared to D is attributed to the higher sputtering yield as a consequence of the higher atomic mass.

The predicted ELM-averaged W sputtering rate in the OVD with a simulated area of 17 m^2 is only 10%–30% lower than in a hypothetical W main chamber with an area of 134 m^2 (figure 6), because the neutral density near the outer divertor entrance and the X-point is elevated by recycled and reflected neutrals from the divertor targets, whereas the recycled neutral flux from the main chamber wall is orders of magnitude lower. The largest W sources contributing to the W contamination of the core plasma are at the OVD (and the MC in the case of a full-W wall), predominantly induced by fuel atoms. Langmuir probe measurements at the OVD indicate that the local ion flux and temperature are too low for ions to significantly contribute to W erosion from the OVD in the studied vertical-horizontal divertor configuration. The ELM-averaged W erosion rate is dominated by the ELM phase contribution in the OVD, but the inter-ELM phase accounts for >80% of the W eroded in the MC region.

The W erosion rate due to atoms at the inner and outer targets is 1–2 orders of magnitude lower than the W erosion rate due to ions. The W screening at both targets is highly effective due to prompt redeposition, SOL ion flows, and the electric field, resulting in a negligible predicted W influx to the confined plasma [7]. Because the PFCs of the OVD do not intersect any flux surfaces near the separatrix, the incident ion flux is negligible compared to the inner and outer targets. Hence, the erosion of the OVD is dominated by atoms rather than ions, and W screening is ineffective near the OVD.

The W erosion rate in the OVD is nearly an order of magnitude higher in the L-mode scenario (figure 6(a)) than during the H-mode inter-ELM phase (figure 6(b)), despite using

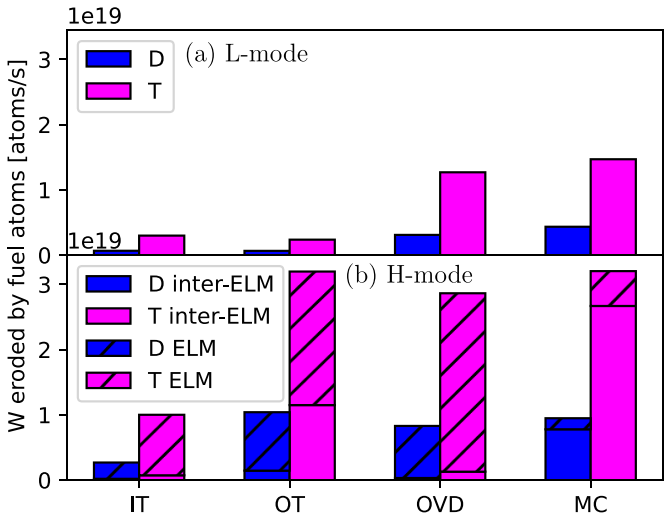

Figure 6. Gross W erosion rate due to incident D (blue) and T (magenta) atoms at the inner target (IT), outer target (OT), outer vertical divertor (OVD) and a hypothetical W main chamber (MC) region of the JET first wall in (a) L-mode #81472 at 9–10 s and (b) H-mode #94606 at 10–11 s. The ELM and inter-ELM contributions in the H-mode scenario are weighted by the relative duration of measured ELM-like and inter-ELM-like heat flux in the SOL (ELM frequency 40 Hz, mean effective ELM duration 2 ms).

only 1 MW of auxiliary heating power compared to 18 MW. The L-mode SOL has a low electron density (8×10^{18} m^{-3} at the mid-plane separatrix), and low-recycling divertor conditions, thus a longer mean free path for CXN from the confined plasma. In contrast, the inter-ELM scenario has several times higher electron density in the SOL, attenuating the flux of energetic CXN from the pedestal region.

3.3. Impact of the CXN distribution on the W radiated power

A hypothetical replacement of all JET plasma-facing materials with W, including the beryllium (Be) limiters, antennas, and the recessed Inconel vacuum vessel wall, is expected to magnify the H-mode ELM-averaged power radiated by W in the core plasma from 6.0 to 12.4 MW (figure 7). After subtracting the experimentally inferred power radiated by Be and medium-Z elements [18] due to impurity influx from the replaced non-W surfaces, the total radiated power by all plasma species in the core is predicted to increase from 8.0 to 12.9 MW. Due to modelling uncertainties, mainly in the simulated plasma conditions and the W cooling factor, the volume-integrated radiated powers predicted by the JINTRAC suite of codes [19] have been rescaled by a factor of 1.8 such that the total radiation in the Be/W JET case is consistent with the tomographic reconstruction of bolometry.

In previous ERO2.0 [20] and JINTRAC simulations of predictive W erosion and transport in JET [7, 11], the assumption of a constant 60° impact angle was applied for sputtering of W by atoms, due to the unavailability of impact angle distributions. Compared to updated predictions based on the energy- and angular-resolved impact distributions from EIRENE, the net effect of the assumed 60° angle is an artificial 17% increase in W density and W radiated power in the core plasma (figure 7).

4. Conclusions

The functional expansion tallying (FET) method was implemented in EIRENE and applied to simulations of the bivariate energy-angular atomic impact spectra in JET L-mode and H-mode plasmas. FET with a Legendre polynomial basis produces atomic spectra with arbitrarily high angular resolution and reduced Monte Carlo noise compared to histogram binning. The JET simulations indicate on average a 10% decrease in W erosion by atoms and W core radiation due to the correlation between the atomic impact energy and angle distributions (research question 1). The measurement uncertainties are too high to determine the W sputtering rate experimentally with $\pm 10\%$ accuracy in any of the studied scenarios.

EIRENE and SDTrimSP6 simulations indicate that the erosion of the non-plasma-wetted W components is higher in T than in D plasmas by up to a factor of 3 in ELMy H-mode, and by up to a factor of 6 during the inter-ELM phase (research question 2). The erosion rate of non-plasma-wetted W surfaces near and above the low-field side divertor entrance is the main cause of the W influx to the core predicted by ERO2.0 [7]. Thus, the dependence of predicted W radiation in the core to the W erosion rate due to the atomic impact distribution in the incompletely screened wall regions is approximately linear in the trace-impurity regime with low impact of W density on the plasma conditions, and stronger than linear if W radiation degrades the screening of W (research question 3). Direct experimental quantification of W erosion by CXN in JET is challenging due to the low W flux density distributed across a large area.

A constant effective impact angle typically in the range 40°–60°, depending on the plasma scenario and the local geometry, is found to be a fair approximation for estimates of W sputtering by CXN if the bivariate energy-angular distribution is unavailable. Applying an appropriately chosen effective impact angle is found to yield more accurate W erosion rates than assuming independent energy and angular distributions.

The choice of only 15 energy bins for the bivariate distribution was driven mainly by the computational cost of obtaining accurate 2D energy-angular histogram tallies to verify the FET results. Higher energy resolution is recommended for simulations using FET without the 2D histograms.

In addition to CXN, incident ions reflected as atoms from PFCs cause sputtering on secondary impact with another surface. The mean energy of the reflected atoms is lower than the impact energy of the original ions, generally resulting in a lower gross erosion yield. Nevertheless, fast reflected atoms are predicted as a significant cause of net erosion of W during ELMs, because the ion impacts inducing the highest gross

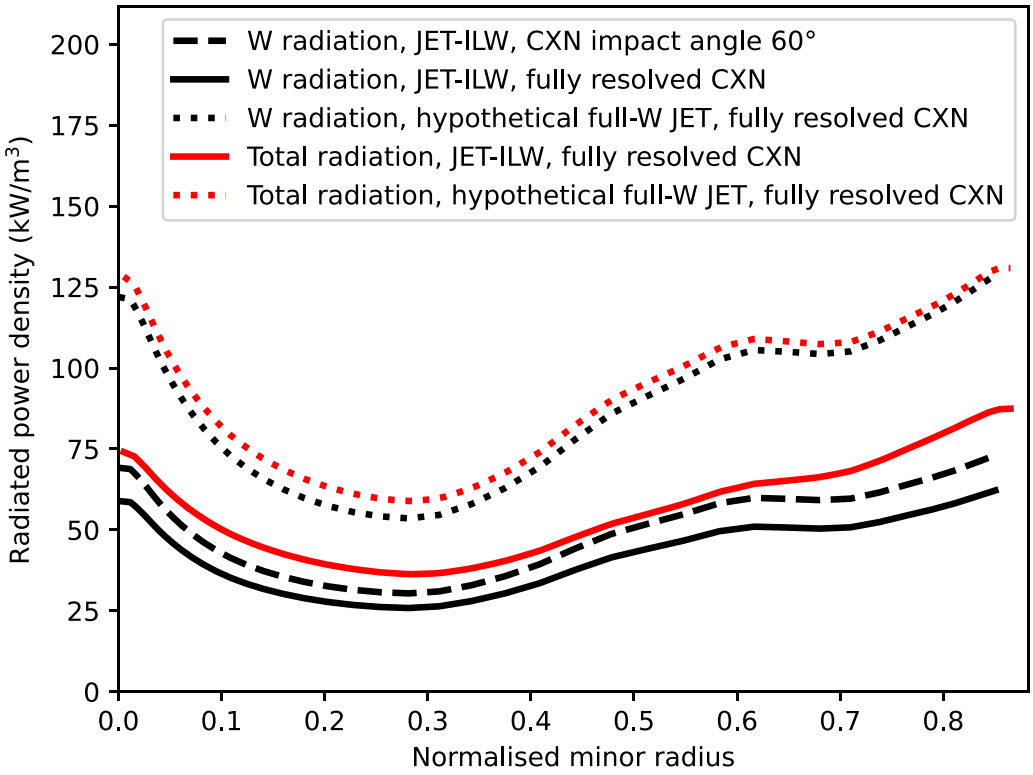

Figure 7. The total ELM-averaged radiated power density and the contribution of W radiation in JET discharge #94606 (deuterium) at 10–11 s based on JINTRAC simulations [7] with varied boundary conditions for W. The full-W JET calculations assume that all Be and Inconel surfaces are replaced with W and that the plasma conditions are maintained constant by offsetting the increased W radiation with additional plasma heating.

erosion rate occur on plasma-wetted surfaces which generally have a very high fraction of prompt and non-prompt local redeposition.

The uncertainty induced by the EDGE2D-EIRENE computational domain not covering the far SOL up to the OVD and main chamber wall is estimated from Thomson scattering and Langmuir probe data to be less than 1%, both for the attenuation of CXN fluxes in the far SOL, and for the total W erosion rate predicted at the OVD. However, in contrast to CXN attenuation and W erosion, W_0 ionization and W ion transport are significantly affected by the far-SOL plasma. This is accounted for in the ERO2.0 simulations [7] used as the basis for figure 7 by extrapolating the plasma conditions radially from the grid boundary to the wall. The extrapolation assumptions are exponentially decaying n_e, T_e, and heat flux profiles with a decay length calculated from the outermost flux surfaces of the EDGE2D-EIRENE solution, and constant extrapolation for the plasma flow velocity and the electric field.

A hypothetical full-W JET would be expected to result in higher but tolerable impurity radiation, within a factor of 2 of the Be/W JET (research question 4, for the cases studied), assuming unchanged SOL conditions and no increase in the oxygen concentration. Plasma scenarios approaching the maximum tolerable W concentration may require further scenario development to avoid runaway W accumulation. To mitigate the erosion of W by CXNs, it is desirable to have a low neutral density in the edge of the confined plasma and a wide, high-density ionizing SOL with ion energies below the W sputtering threshold.

Data availability statement

The data cannot be made publicly available upon publication because they are not available in a format that is sufficiently accessible or reusable by other researchers. The data that support the findings of this study are available upon reasonable request from the authors.

Acknowledgments

This work is financially supported by a research grant awarded by the Finnish Cultural Foundation.

This work has been carried out within the framework of the EUROfusion Consortium, funded by the European Union via the Euratom Research and Training Programme (Grant Agreement No 101052200—EUROfusion). Views and

opinions expressed are however those of the author(s) only and do not necessarily reflect those of the European Union or the European Commission. Neither the European Union nor the European Commission can be held responsible for them.

ORCID iDs

H A Kumpulainen https://orcid.org/0000-0003-1301-0497
S Brezinsek https://orcid.org/0000-0002-7213-3326
M Groth https://orcid.org/0000-0001-7397-1586
J Romazanov https://orcid.org/0000-0001-9439-786X
S Wiesen https://orcid.org/0000-0002-3696-5475

References

[1] Rapp J *et al* 2017 *Fusion Sci. Technol.* **72** 211–21
[2] Brezinsek S *et al* 2019 *Nucl. Fusion* **59** 096035
[3] Widdowson A *et al* 2019 *Nucl. Mater. Energy* **19** 218–24
[4] Aho-Mantila L *et al* 2013 *J. Nucl. Mater.* **438** S321–5
[5] Yoshida N *et al* 1998 *J. Nucl. Mater.* **258–263** 173–82
[6] Staudenmaier G *et al* 1989 *J. Nucl. Mater.* **162–164** 414–8
[7] Kumpulainen H A *et al* 2024 *Plasma Phys. Control. Fusion* **66** 055007
[8] Barabaschi P *et al* 2025 *Fusion Eng. Des.* **215** 114990
[9] Ongena J *et al* 2024 *21st Int. Congress on Plasma Physics (Tu.Po.8)*
[10] Kumpulainen H A *et al* 2020 *Nucl. Mater. Energy* **25** 100866
[11] Kumpulainen H A *et al* 2022 *Nucl. Mater. Energy* **33** 101264
[12] Simonini R *et al* 1994 *Contrib. Plasma Phys.* **34** 368–73
[13] Reiter D *et al* 2005 *Fusion Sci. Technol.* **47** 172
[14] Rode S *et al* 2024 *Nucl. Mater. Energy* **38** 101564
[15] Griesheimer D 2005 *Doctoral thesis* University of Michigan
[16] Wang Z *et al* 2021 *Nucl. Eng. Technol.* **53** 430–8
[17] Mutzke A et al 2019 SDTrimSP version 6.00 IPP-Report 2019-02
[18] Sertoli M *et al* 2019 *J. Plasma Phys.* **85** 90585050
[19] Romanelli M *et al* 2014 *Plasma Fusion Res.* **9** 3403023
[20] Romazanov J *et al* 2019 *Nucl. Mater. Energy* **18** 331–8